doi:10.1016/j.jmb.2004.12.015 J. Mol. Biol. (2005) 346, 815–831

JMB

Available online at www.sciencedirect.com

SCIENCE DIRECT®

ELSEVIER

Crystallographic Structure of the $T=1$ Particle of Brome Mosaic Virus

Steven B. Larson, Robert W. Lucas and Alexander McPherson*

Department of Molecular Biology and Biochemistry University of California, Irvine CA 92697-3900, USA

**Corresponding author*

$T=1$ icosahedral particles of amino terminally truncated brome mosaic virus (BMV) protein were created by treatment of the wild-type $T=3$ virus with 1 M $CaCl_2$ and crystallized from sodium malonate. Diffraction data were collected from frozen crystals to beyond 2.9 Å resolution and the structure determined by molecular replacement and phase extension. The particles are composed of pentameric capsomeres from the wild-type virions which have reoriented with respect to the original particle pentameric axes by rotations of 37°, and formed tenuous interactions with one another, principally through conformationally altered C-terminal polypeptides. Otherwise, the pentamers are virtually superimposable upon those of the original $T=3$ BMV particles. The $T=1$ particles, in the crystals, are not perfect icosahedra, but deviate slightly from exact symmetry, possibly due to packing interactions. This suggests that the $T=1$ particles are deformable, which is consistent with the loose arrangement of pentamers and latticework of holes that penetrate the surface. Atomic force microscopy showed that the $T=3$ to $T=1$ transition could occur by shedding of hexameric capsomeres and restructuring of remaining pentamers accompanied by direct condensation. Knowledge of the structures of the BMV wild-type and $T=1$ particles now permit us to propose a tentative model for that process. A comparison of the BMV $T=1$ particles was made with the reassembled $T=1$ particles produced from the coat protein of trypsin treated alfalfa mosaic virus (AlMV), another bromovirus. There is little resemblance between the two particles. The BMV particle, with a maximum diameter of 195 Å, is made from distinctive pentameric capsomeres with large holes along the 3-fold axis, while the AlMV particle, of approximate maximum diameter 220 Å, has subunits closely packed around the 3-fold axis, large holes along the 5-fold axis, and few contacts within pentamers. In both particles crucial linkages are made about icosahedral dyads.

Keywords: structural transition; proteolysis; AlMV; symmetry; assembly

Introduction

There are several examples of plant virus coat proteins normally found in $T=3$ capsids that can be made to reassemble *in vitro* into discrete $T=1$ icosahedral particles. The principal requirement for reassembly appears to be the proteolytic cleavage and release of extended, N-terminal polypeptides. The lost peptides, which are essential for encapsidation of nucleic acid,[1,2] contain many basic amino acid residues, are strongly positively charged, and are primarily responsible for tethering the capsid protein to the genomic RNA at the core of the particle.

$T=3$ icosahedral viruses whose coat proteins exhibit that behavior are brome mosaic virus (BMV), alfalfa mosaic virus (AlMV), sesbania mosaic virus (SeMV), and southern bean mosaic virus (SBMV). Both SeMV and SBMV belong to the sobemovirus genus, BMV is the type strain of the bromovirus genus, and some controversy remains

Abbreviations used: BMV, brome mosaic virus; AlMV, alfalfa mosaic virus; SeMV, sesbania mosaic virus; SBMV, southern bean mosaic virus; AFM, atomic force microscopy; MR, molecular replacement; SA, simulated annealing; ASA, accessible surface area; CC, correlation coefficient.

E-mail address of the corresponding author: amcphers@uci.edu

as to whether AlMV is a bromovirus[3,4] or belongs in the ilarvirus genus.[5,6]

The structures of SBMV, SeMV, and AlMV have been determined crystallographically[4,7–13] though only coordinates for AlMV are currently available. The structure of the AlMV $T=1$ particle was solved only to 4 Å resolution and no definitive placement of amino acid residues was possible. AlMV, however, provides the most relevant comparison because its properties are somewhat similar to BMV, and most taxonomy places it in the same genus.[3,4]

Table 1 describes the capsid protein properties and the cleavages created by proteolysis that lead to reassembly into $T=1$ particles. To produce the $T=1$ particles of SBMV and AlMV, the capsid protein was exposed to trypsin;[4,6,7,9] for SeMV, recombinant proteins of two different lengths were reassembled;[10,11] and for BMV, $T=1$ particles formed after cleavage of the native coat protein by, presumably, endogenous proteases.[14]

We previously reported the *in vitro* reassembly of the coat protein of BMV into $T=1$ particles after loss of 35 amino acid residues from the N terminus, as well as its crystallization for X-ray diffraction analysis.[14] In that investigation, no exogenous protease was added and the cleavage, apparently, was produced by endogenous enzymes present in the preparation. It was earlier reported by others, however, that $T=1$ particles of BMV could also be prepared by treatment of BMV with trypsin and the loss of 63 amino acid residues from the N terminus.[15,16] The dissociated protein of both BMV and AlMV, as well as the trypsinized forms, have also been reported to form other reassembly products such as tubes, helices, double shelled particles, empty capsids, and sheets.[17–19]

In addition to initiating an X-ray diffraction analysis of both the native $T=3$ BMV virions and the $T=1$ particles, we previously described an *in situ* atomic force microscopy (AFM) investigation to visualize the transformation of $T=3$ into $T=1$ particles in the presence of high concentrations of $CaCl_2$.[14] The study demonstrated that, at least in some cases, $T=3$ virions could condense directly into $T=1$ particles without undergoing complete dissociation, and that this transformation was likely accompanied by the shedding of hexameric capsomeres. That is, as hexameric clusters dissociated from the virions, the pentameric capsomeres appeared to spontaneously reorganize within the capsid of the disintegrating virions into $T=1$ icosahedra. Complete dissociation of $T=3$ virions into individual capsomeres, dimers or protein subunits, and subsequent reassembly into $T=1$ particles may proceed as well, but the AFM results demonstrate that the former process can, and does, occur.

BMV is the type strain of the bromoviridae[20,21] and has a multipartite genome of four separate, single stranded RNA molecules that code for at least four proteins, including the capsid protein. RNA1 and RNA2 are encapsidated in separate but otherwise identical $T=3$ icosahedral particles, and the pair RNA3 plus RNA4 (a subgenomic fragment of RNA3 which codes for the coat protein) in another.[22] The virions are about 280 Å in diameter[23] and the structure of the native $T=3$ particle has been solved in this laboratory by X-ray crystallography.[24] BMV virions are frequently characterized structurally as being rather loose assemblies that depend upon protein–nucleic acid interactions and divalent cations to maintain their integrity.[24,25,26] Indeed, Mg^{2+} on quasi-3-fold axes coordinated to three quasi-symmetrically equivalent aspartic acid residues are observed in the native structure. Pentameric and hexameric capsomeres are otherwise rather loosely associated.

A prominent and extensively studied feature of BMV is that it undergoes a reversible structural transition at moderate (0.5 M NaCl) salt concentration between pH 6 and pH 7.[25] This results in an RNase and protease sensitive particle whose diameter is about 15% greater than the original (310 Å *versus* 268 Å, as determined by small-angle scattering).[23,27,28] While this pH-promoted transition is suppressed to some extent by Mg^{2+}, at high-salt concentrations and pH 7 or higher, the virions dissociate into free protein and protein–nucleic acid complexes.[15,29,30] RNA is lost, and the N-terminal polypeptides become susceptible to proteolysis.

We describe here the structure solution by X-ray crystallography of the BMV $T=1$ particle in a tetragonal unit cell. By comparison with the wild-type virion, the $T=1$ particle structure lends some insight into how $T=3$ virions may transform into $T=1$ particles. Comparison with the $T=1$ particle of AlMV shows very little similarity in their structures and, in fact, suggests that the modes and mechanisms of reassembly are quite different. In both cases, however, residual architectural elements of the structures of the native $T=3$ virions persist.

Results

More than 20 sets of diffraction data were

Table 1. Various physical properties associated with the four viruses possessing the capacity to form $T=1$ particles

	SBMV	SeMV	AlMV	BMV
Native capsid protein M_r	28,214	29,000	24,238	20,346
Number of residues	279	268	220	189
Number of residues removed	61	36/65	26	35
$T=1$ coat protein Mr	22,000	25,000/16,900	21,400	16,450
Number of residues	218	232/203	194	154

collected from crystals of the $T=1$ particles of BMV, and though the crystals appeared morphologically the same, at least four different crystallographic unit cells were observed. These were all tetragonal but either differed by doublings of unit cell edge dimensions, or the presence or absence of symmetry elements perpendicular to the tetragonal axis. A further report on the other unit cells will be given elsewhere, as the present analysis focuses on the crystal form yielding the most consistent cell dimensions, best comparison (R_{merge}) of equivalent data from different crystals, and which diffracted to the highest resolution. This had unit cell dimensions of $a=b=195$ Å, $c=429$ Å, and $Z=4$. For the structure determination described here, data from a single frozen crystal were used.

Space group and structure determination

The process of space group and structure determination is diagrammed in Figure 1. The marginal difference in R_{merge} between Laue groups 4/mmm and 4/m (0.153 *versus* 0.118) and the initial orientation obtained from self-rotation functions suggested that the space group was $P4_122$ (or $P4_322$) with a particle on the y-axis near $y=½$ and an interparticle distance of ~175 Å. A molecular replacement (MR) search using a pentamer of the native BMV model as probe produced a model in which the pentamer was rotated 37° about the 5-fold axis and radially contracted along that axis to a mean $T=1$ particle diameter of 150 Å. A crystallographically unique, icosahedrally constrained hemisphere of six pentamers was constructed. The position and orientation of this model were refined by translation along and rotation about the y-axis in both $P4_122$ and $P4_322$ with essentially the equivalent results of CC = 0.35 and $R=0.50$. Phase extension in both space groups, starting from the corresponding model phases to 10 Å resolution, was disappointing and was, therefore, halted below 5 Å resolution.

Expanding the hemisphere model to a full icosahedrally constrained sphere of 12 pentamers, the MR search was repeated in space groups $P4_1$ and $P4_3$ except that a two-dimensional translation search in the x and y-directions was done in addition to rotation about the y-direction. The resulting CC = 0.59 and $R=0.44$ for $P4_3$ *versus* CC = 0.36 and $R=0.50$ for $P4_1$ clearly showed $P4_3$ to be the correct space group. This refined model provided the initial phases to 10 Å resolution for phase extension to 3 Å using NCS map averaging and solvent flattening in space group $P4_3$. The results of the phase extension are plotted in Figure 2.

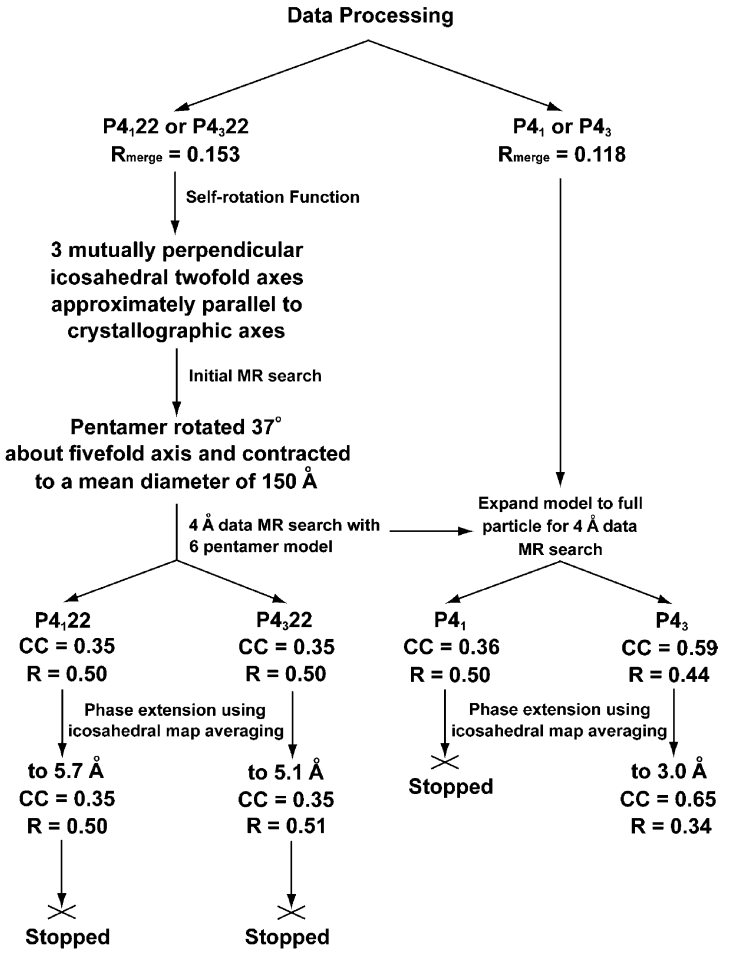

Figure 1. Schematic diagram of the structure solution process.

Structure refinement

Using an electron density map calculated with 3 Å phases from phase extension, the model was rebuilt and attempts were made to refine it by simulated annealing (SA). This, however, proved unsuccessful with both R and R_{free} immobilized at 0.35. At this point icosahedral symmetry was relaxed, since, indeed, there was no crystallographic constraint on the particles that required any symmetry element of icosahedral symmetry. Thirty cycles of 60-body rigid-body refinement against 3.3 Å data immediately precipitated a drop in the conventional R-factor to 0.263 and R_{free} to 0.277. We would have been cautious of this result had the R_{free} not fallen by 22%, as relaxation of constraints might normally be expected to improve agreement between calculated and observed structure amplitudes. The reduction in R_{free} implied that the improvement was not simply a case of over fitting.

The results from phase extension using strict icosahedral NCS, although indicative of the correct space group and a good starting model, had been disappointing. Therefore, we determined the quasi-icosahedral NCS operators between one subunit and the other 59 subunits of the rigid body model. Starting from a 10 Å phase set based on the 60 subunits of the rigid body model, phase extension to 3 Å was performed by map averaging with the quasi-icosahedral NCS operators. The results, shown in Figure 2, demonstrate the superiority of the quasi-icosahedral NCS model over the icosahedral model, especially at higher resolution. The results are reminiscent of correctly performed phase extension procedures for viruses and are comparable to our results with other virus structural analyses.[24,31–34]

During the analysis of the particle asymmetry that is described below, it was discovered that a nearly exact 2-fold axis, parallel with the crystallographic x-axis, did exist between specific orientations of twofold related pentamers. After reorienting the model to bring this axis coincident with the crystallographic y-axis and eliminating the twofold related pentamers, the model was refined in space group $P4_322$ producing comparable results to the $P4_3$ model refinement. Thus, the correct space group is $P4_322$.

The model

The model, composed of 30 subunits of 154 amino acid residues and 15 water molecules per subunit, was alternately rebuilt and refined by SA in space group $P4_322$ using NCS restraints to a final R at 2.9 Å of 0.219 and R_{free} of 0.239. Selected model statistics are presented in Table 2. Figure 3 illustrates the quality and resolution of the electron density on which the model is based. As suggested by the mean thermal parameters of the N and C-terminal polypeptides (residues 36–39 and 187–189, respectively), the electron density in these

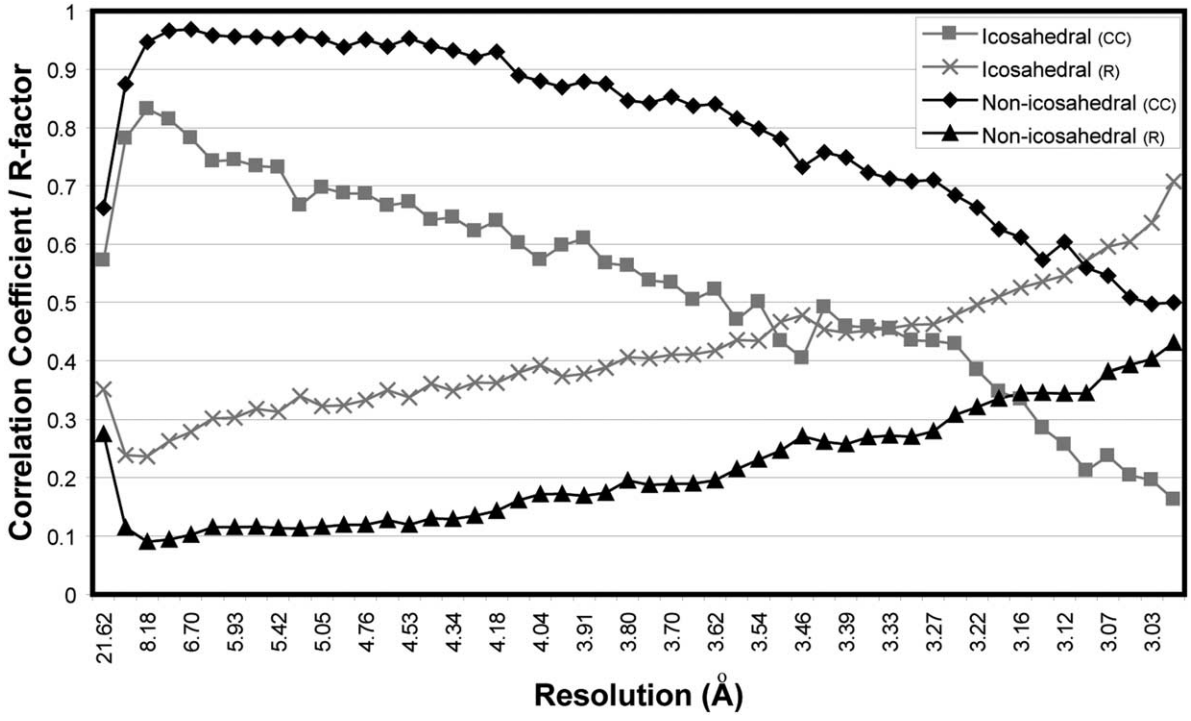

Figure 2. Plot of correlation coefficient and R-factor *versus* resolution for the final cycle of phase extension using both icosahedral non-crystallographic symmetry averaging (CC = ■, R = ×) and quasi-icosahedral NCS averaging (CC = ♦ R = ▲).

Table 2. Refinement and model statistics for $T=1$ BMV

	Protein	Water
Residues/molecules	4620	450
Residues or molecules/subunit	154	15
Atoms	34,800	450
$\langle B \rangle$ (Å^2)	63.6	53.6
B_{min} (Å^2)	20.2	10.9
B_{max} (Å^2)	131.5	100.6

NCS restraints applied in 5 groups		$\langle B \rangle$
Group 1: all atoms of residues 48–177	Weight = 120 kcal/mol	61.2 Å^2
Group 2: all atoms of residues 40–47	Weight = 20 kcal/mol	65.7 Å^2
Group 3: all atoms of residues 178–186	Weight = 20 kcal/mol	65.1 Å^2
Group 4: all atoms of residues 36–39	Weight = 0 kcal/mol	115.7 Å^2
Group 5: all atoms of residues 187–189	Weight = 0 kcal/mol	91.9 Å^2
(Note: weight = 0 implies no restraints)		

RMS deviations from ideal geometry	
Bonds (Å)	0.010
Angles (°)	1.42
Dihedrals (°)	25.80
Impropers (°)	0.77

Ramachandran plot summary		
Most favored region	3584 residues	85.9%
Additionally allowed region	542 residues	13.0%
Generously allowed region	42 residues	1.0%
Disallowed region	2 residues	0.1%
Total	4170 residues	100.0%

$R = 0.219$, $R_{free} = 0.239$ for 157,521 reflections with $F \geq 1.1\sigma_F$ (86.5% of the data).

regions, although present, is poorly defined, especially for side-chain atoms; however, no atoms were assigned zero occupancy. Of the 44 residues in the generously allowed or disallowed regions of the Ramachandran plot, 15 are in the N and C termini. There are only five non-equivalent residues in these 44; these are (with number of occurrences in parentheses): Ala37 (9), Gln39 (4), Lys64 (18), Lys165 (11), and Tyr188 (2). Lys64 is in the β-hairpin BC loop. For the purposes of discussion, the 30 subunits in the model will be identified as six pentamers, labeled A through F, with the five subunits in each pentamer numbered 1–5, as diagrammed in Figure 4. Throughout this paper, superposing of subunits and the calculation of centroids and RMS deviations will be based on the C^{α} atoms of residues 41–181, unless otherwise noted. Pair wise superposing of the 30 subunits (435 combinations) produces a mean RMS deviation of 0.13 Å (0.16 Å for all atoms in this region). It should be noted that all these residues were in one of the three restraint groups during refinement. By contrast, the N termini (residues 36–40) and C termini (residues 182–189) have mean RMS deviations of 4.36 Å and 1.73 Å, respectively. Clearly, variability of the N and C termini, suggested by *B*-factors and map density, is confirmed.

Comparison to native *T*=3 BMV

The subunits of the $T=1$ particle are nearly identical with the subunits of the $T=3$ native virion, except for the N and C termini. Superposition of subunits A, B, and C of the $T=3$ model onto the 30 $T=1$ subunits shows that the β-barrel cores (mean RMSD = 1.14 Å) are very similar while the N and C termini (mean RMSD = 12.25 Å and 9.06 Å, respectively) are very distinct, indicating that a substantial change in these terminal polypeptides took place during the transition from a $T=3$ virion to a $T=1$ particle. The superposition of the three $T=3$ subunits onto subunit A1 of the $T=1$ particle is shown in Figure 5. It should be pointed out that the resolution of the structure determination of the $T=1$ particle was 2.9 Å, while that for the native BMV was a nominal 3.7 Å.[24] Thus, we might expect the $T=1$ subunit structure in the present study to be more precise. Indeed, although the statistics for bonds and angles are similar between the $T=1$ and the native model, the percentage of residues in the most favored regions of the Ramachandran plot (calculated with PROCHECK[35] is 86% for the former *versus* only 68% for the latter.

The six unique pentamers of the $T=1$ particles are virtually identical with the pentameric capsomeres in the native particle, again with the exception of the N and C-terminal peptides. The average RMS deviation between the C_{α} atoms of the $T=1$ pentamers with the native pentamer (excluding N and C-terminal residues) is 1.15 Å, the same for single subunits (range: 1.14–1.17 Å). This is not unexpected if the $T=1$ particles are

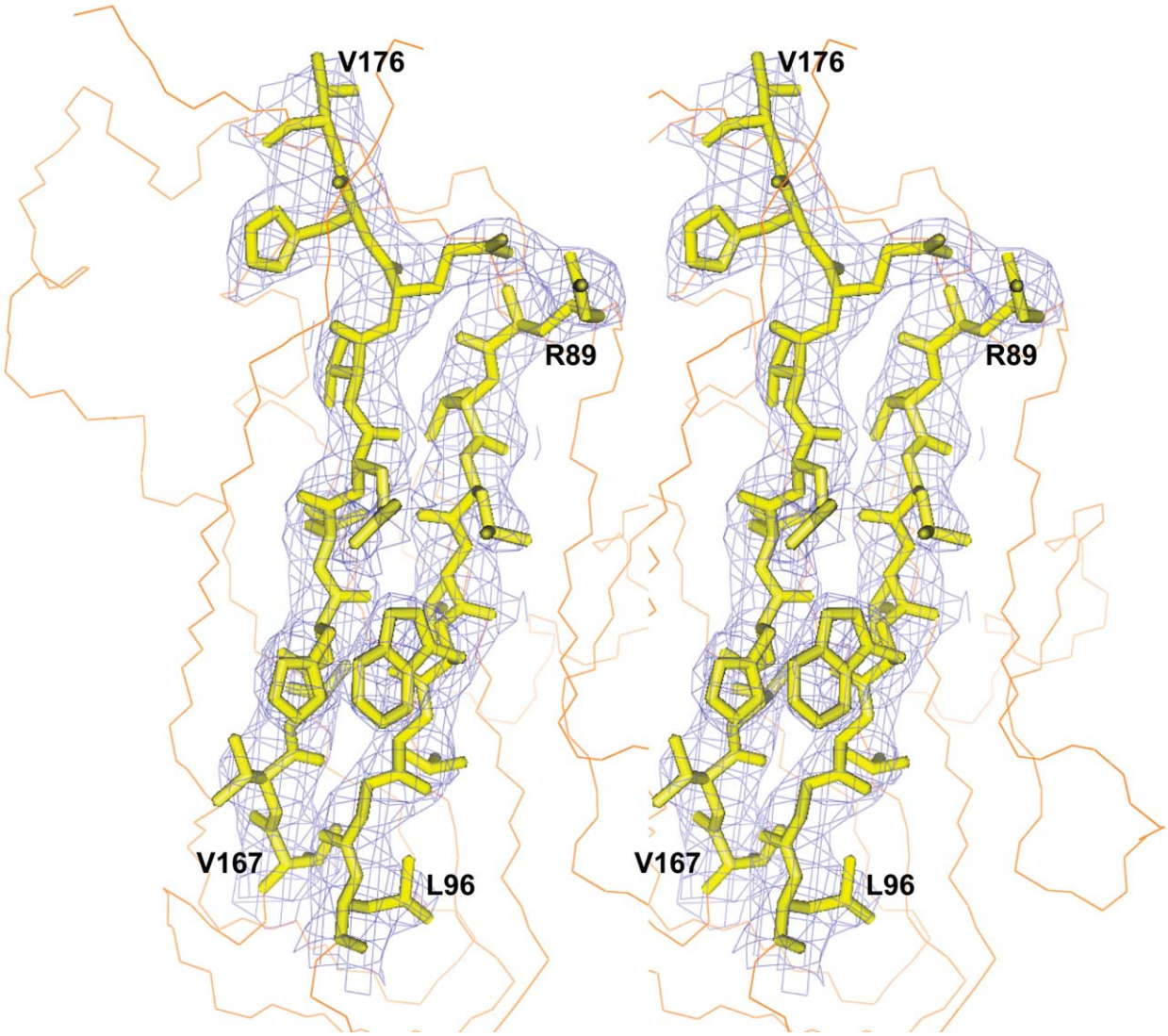

Figure 3. A stereo view of the electron density from a 3.0 Å resolution Fourier map utilizing phases obtained from the phase extension process. Density is contoured at 1.2σ and covers adjacent strands of the eight stranded β-barrel containing residues 89–96 and 167–176. The remainder of the subunit is rendered as a main-chain tracing.

formed from disintegrating $T=3$ virions by direct condensation, as indicated by the earlier AFM studies.[14] It is quite clear from the structures that the $T=1$ particle is indeed formed from native, pentameric units. The pentamers undergo a rotation of 37° with respect to their orientation in the $T=3$ particle, and during transformation move from a mean radius of 113 Å in the native $T=3$ virion (or about 130 Å in the swollen virion) to 75 Å in the $T=1$ particle.

The pair wise relationships of subunits (defined in Figure 6) in the $T=1$ particle were compared to the relationships of equivalent subunits in the $T=3$ virion by superposing a subunit of the latter onto the equivalent subunit of each of the subunits in the $T=1$ particle followed by superposition of the $T=3$ paired subunit onto its equivalent $T=1$ subunit. The translation and rotation of the paired subunit is a measure of the change in these pair-wise relationships during the transformation from the $T=3$ virion to the $T=1$ particle. These results are presented in Table 3, along with the results for similar calculations for the sesbania mosaic virus $T=3$ and $T=1$ particles. Whereas, there is a single calculation for each interaction in the SeMV case, there are 30 calculations for each interaction in the BMV case. As has been noted, the pentameric relationship changed little between the $T=3$ and $T=1$ particles. However, the dimer and trimer relationships are very distinct. In the SeMV case, the only extreme change in subunit interactions occurred in the true dimer pair. In BMV, the true dimer pair (the pentameric pair aside) experiences the least change. It is obvious that all relationships (except between pentameric subunits) undergo an extreme separation as indicated by the residual translations, which for most subunits is greater than 10 Å.

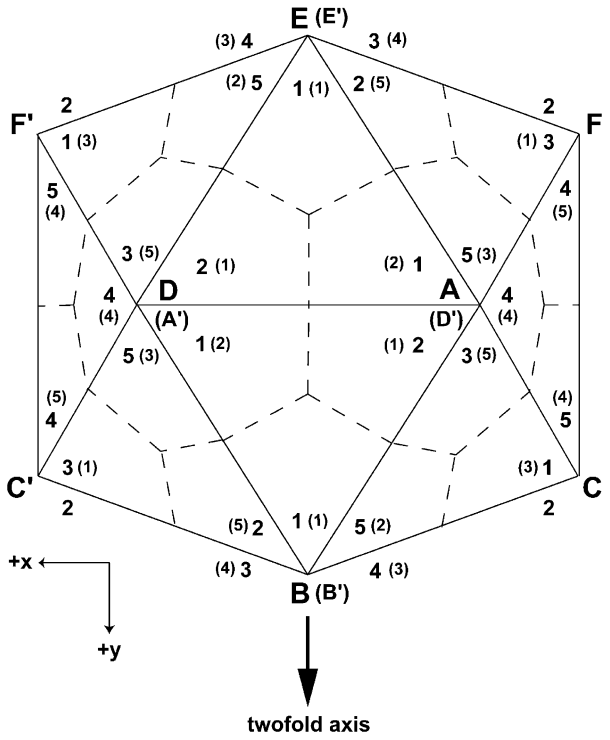

Figure 4. Schematic diagram illustrating how subunits are identified. The six pentamers in the asymmetric unit are labeled A through F and the five subunits in each pentamer are numbered 1 through 5. Hence, the first subunit is A1. Twofold equivalent pentamers are A′ through F′. Pentamers C, C′, F, and F′ are in the plane of the page. Pentamers and subunits below the plane (underside of the particle) are in parentheses.

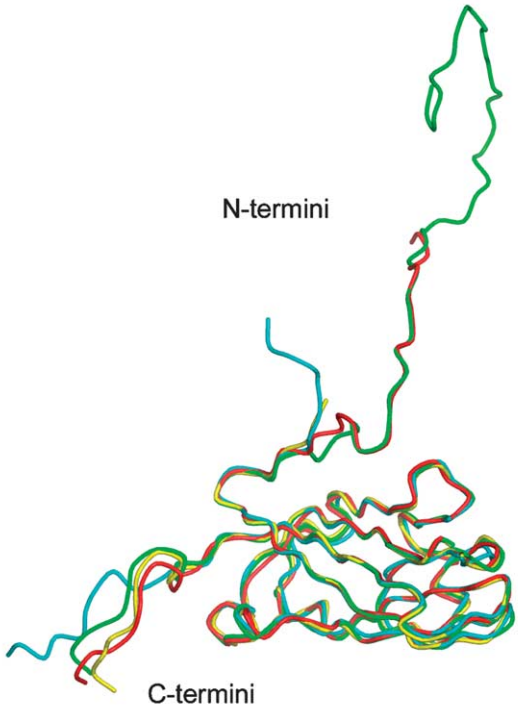

Figure 5. Superposition of subunits A (yellow), B (red) and C (green) of the intact BMV virion onto a subunit of the $T=1$ BMV particle (cyan). A least-squares fit of 141 C^{α} atoms of the β-barrel of the respective subunits gave an RMS deviation of 1.09 Å for the A subunit, 1.17 Å for the B subunit, and 1.17 Å for the C subunit.

The quasi-icosahedral $T=1$ particle structure

The $T=1$ BMV particle has a mean diameter of about 150 Å (maximum diameter is ~195 Å). Figure 7 and the results in Table 3 suggest that the capsomeres are loosely bound through the C-terminal peptides. The extent of the union between pentamers may best be illustrated by the amount of surface area buried in the formation of these interactions. The isolated subunits have an average accessible surface area (ASA) of 9549 $Å^2$. In the presence of the other members of its pentamer the ASA is reduced to 8253 $Å^2$ for a net average loss of 1296 $Å^2$ per monomer. When a subunit binds to another in an adjacent pentamer through the C-terminal strands, the ASA is reduced to 6192 $Å^2$, an average loss of 2061 $Å^2$. This would suggest that inter-pentameric interactions, in the complete particle, are in fact more extensive than intra-pentameric interactions. However, the principle source of this strength may lie in the very ends of the C terminus with otherwise only tenuous linkages between pentamers.

The interior of the particle contains a lumen of about 85–90 Å in diameter. This is somewhat smaller than that found in the satellite plant viruses[36] by about 10 Å, but could easily accommodate at least 1000 nucleotides. In difference Fourier maps, however, we observe no evidence of RNA fragments binding to the inside of the capsid. There was also none observed, however, in the native virion. The $T=1$ capsid is penetrated by large holes along the 3-fold axis, and indeed, the entire protein surface network appears remarkably open and tenuously maintained. Small molecules and perhaps even small proteins could penetrate the interior. The $T=3$ virions of native BMV were maintained in part by Mg^{2+} located on the quasi 3-fold axis of the icosahedrons.[24] We find no evidence in difference Fourier maps for the presence of any divalent ions in the $T=1$ particles.

The nature of the breakdown of icosahedral symmetry can be viewed in various ways. Since the structure was initially solved as an icosahedral particle, the final quasi-icosahedral particle model can be compared to the last icosahedral model. Clearly, the pentamers are fairly stable entities as shown by the consistency between the native pentamer and the $T=1$ pentamers. This was further substantiated by comparison of the six crystallographically unique $T=1$ pentamers to one another in each of the five different orientations, for example pentamer A was superimposed onto pentamer B, first with subunit A1 onto B1, then with

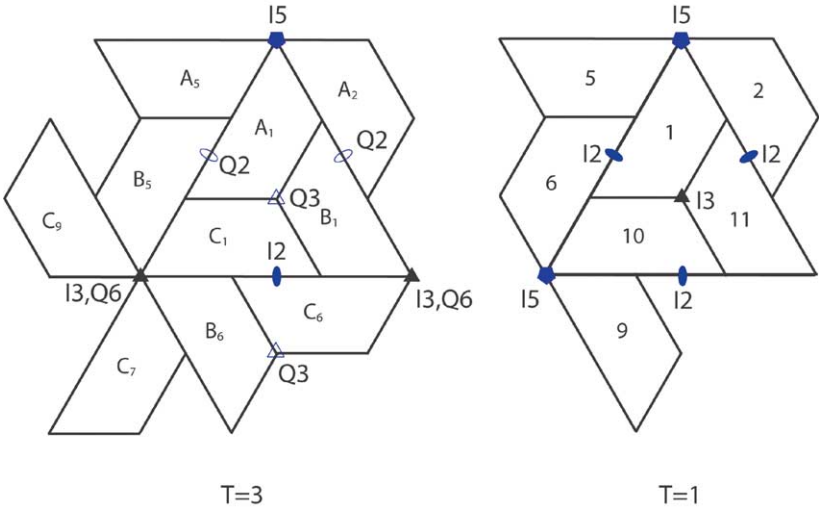

Figure 6. $T=3$ and $T=1$ subunit nomenclature. The icosahedral asymmetric unit for $T=3$ viruses is three chemically equivalent subunits (A, B, and C). Symbols for exact symmetry axes are solid black and labeled I2, I3, or I5; symbols for quasi symmetry axes are white and labeled Q2, Q3 and Q6.

A1 onto B2, then A1 onto B3, etc. There are 75 such combinations and the RMS deviations ranged from 0.22 Å to 0.44 Å. Thus, it seems reasonable to look at the distortions as a movement of pentamers rather than individual subunits, which seem to maintain a constant relationship within the pentameric capsomeres. Diagrammatically, this has been done in Figure 8, which illustrates the overall change from icosahedral symmetry. There appears to be a counter-clockwise rotation of subunits around the 5-fold axis of the pentamer in the foreground. The superposition of the icosahedral model onto the quasi-icosahedral model produces a minimal change in the position and orientation, the rotation is 0.07° and the translation is 0.003 Å. The RMS deviation between the two models is only 1.03 Å. The superposition of each pentamer of the icosahedral model onto the equivalent pentamer of the quasi-icosahedral model produces moderately larger changes with translations in the range of 0.29 Å to 1.14 Å and rotations of 1–2° (see Table 4).

The spatial relationships in the $T=1$ particle are diagrammed in Figure 9 and summarized in Table 4. Analyzing the distribution of pentamers in the capsid, we find that pentamer B moved the most (1.14 Å), which resulted in the shortest inter-pentamer distances of 73.9 Å, 74.5 Å, and 74.5 Å for the B–B′, B–C′ and B–D pairs. Except for the A–E distance of 76.1 Å, all other inter-pentamer distances are close to the icosahedral value of 75.2 Å. Except for pentamer B, which has a radius of only 70.6 Å, the pentamer radii are within 0.5 Å of the icosahedral value of ~71.5 Å. Perhaps the greatest deviation from icosahedral symmetry results from the tilting of pentamers with respect to the original icosahedral 5-fold axes. Clearly, the vectors between pentamer centroids and the center of the particle very closely align with the icosahedral axis, as indicated by the narrow range of angles between them. This is in contrast to the wide range of inter-axial angles based on the calculated pentameric 5-fold axes. This wide range results from 5-fold axes not passing through the center of the particle because of the tilt of the pentamers. Thus, from Figure 9, we could surmise that pentamers A, E and F tilt towards each other to some degree because all three inter-axial angles are considerably greater than the icosahedral ideal. The range of radii of subunits within each pentamer (see Table 4(D)) is also a manifestation of the pentamer tilt. Pentamer F contains subunits at a radius of 74.2 Å and 75.9 Å, the largest range of any pentamer, and it also had the largest rotation of 2.2°. Lastly, the rotation axis for the superposition calculations (Table 4(A)) for every pentamer except B are axes that are nearly perpendicular to the original icosahedral 5-fold axes, and, therefore, produce tilted pentamers with respect to those 5-fold axes. Pentamer tilts of 2° translate into a 2 Å difference in the distance from the particle center for equivalent atoms on opposite sides of the pentamer, 30 Å from its center.

Thus, the $T=1$ BMV particle has a nearly perfect icosahedral framework from a spatial distribution point of view, except that it is slightly twisted (as seen in Figure 8); all pentamers have some tilt with respect to the original icosahedral 5-fold axes; and, some pentamers have contracted (minimum radius of 70.6 Å for pentamer B) and some have expanded (maximum radius of 72.0 Å for pentamer C) with respect to the particle center.

Packing interactions

$T=1$ particles pack in the lattice surrounded by eight nearest neighbor particles such that the interface between two particles involves three pentamers from each particle. The particle is rotated about the *y*-axis such that a quasi-2-fold axis of the particle is approximately 3.4° from the crystallographic *y*–*z* plane. Table 5 lists the pentamers, subunits and residues that make up the four unique interfaces based on a maximum 4 Å contact distance. These interactions mainly involve

Table 3. Relative change in disposition of subunits from the native $T=3$ virions and the $T=1$ particles for BMV and SeMV (see Figure 6)

Pair in $T=3$ ($T=1$) particle	BMV		BMV		SeMV CP NΔ36		SeMV CP NΔ65		
	Mean rotation (°)	Mean translation	Rotation range	Translation range (Å)	Rotation (°)	Translation (Å)	Rotation (°)	Translation (Å)	Subunit icosahedral relationship
A_1/A_5 (1/5)	1.43°	0.50 Å	0.6–2.6	0.2–0.8	2.2	0.20	2.1	0.11	Pentamer
A_1/B_1 (1/11)	18.02	11.39	15.2–23.4	9.6–13.7	3.6	0.22	3.8	0.05	Trimer
A_1/C_1 (1/10)	25.56	12.90	22.5–30.8	11.5–15.7	5.7	0.14	5.8	0.11	Trimer
A_1/B_5 (1/6)	17.10	11.08	14.7–22.9	9.7–13.4	4.6	0.42	4.7	0.51	Dimer
C_1/C_6 (1/6)	7.41	8.16	4.9–12.9	6.8–10.4	38.4	2.31	38.4	2.23	Dimer

The first subunit of the $T=3$ subunit pair was superimposed on the corresponding subunit of the $T=1$ particle and the residual rotation and translation of the second subunit of the pair was obtained by superposing the $T=3$ subunit onto the corresponding subunit of the $T=1$ particle, translation being the distance between the subunit centroids before and after the superposition.

residues in the BC, the DE, and the EF loops and β-strand I and are symmetric across the interfaces for the A–B–C/A′–B′–C′ and D–E–F′/D′–E′–F interfaces. The other two interfaces are equivalent to each other but the interactions are not symmetric across the interfaces. Only 26 of the 60 subunits in the particle are involved in inter-particle contacts.

Comparison to AlMV

An attempt was made to compare in a quantitative fashion the structure of the BMV subunit with that of AlMV deduced at 4 Å resolution from the $T=1$ particle of AlMV.[4] A sequence comparison (using a BLAST search of the PIR-NREF website)[37] showed almost no identity, and rather little homology, between the coat proteins. It further proved very difficult to superimpose the three-dimensional structures of the coat protein subunits of the two. Because only alpha carbon coordinates were available for AlMV, the comparison had to be carried out at that level. Although both the BMV and the AlMV subunits are constructed around canonical eight-stranded Swiss roll β barrel domains, the sizes and overall shapes of the two were so different that no meaningful superposition could be obtained. It is, therefore, not surprising that the $T=1$ particles of AlMV and BMV are so dissimilar in architecture.

Figure 10 shows the $T=1$ particles of AlMV and BMV viewed along dyad axes. The differences in the particle structures are obvious. First of all, the sizes of the two particles are considerably different. For AlMV the maximum exterior feature is at a diameter of 220.1 Å (using only C^{α} atoms), the mean diameter is 167 Å, and the inside of the shell has a 117 Å diameter. The same measures for the $T=1$ BMV particle are 195 Å, 150 Å, and 88 Å, respectively. Although the BMV pentamers protrude perceptibly, the subunits of the AlMV particles appear to be standing even more "on end" and extend radially even further. It is apparent from Figure 10 that in AlMV there are also extensive interactions about the dyad axes that likely even exceed those in the BMV particle. This is consistent with the observation that complete dissociation of native AlMV virions produces chiefly protein dimers in solution,[5,26] while dissociation of BMV yields pentamers and hexamers[14,30] or monomers.[18,29]

In the BMV $T=1$ particles, there are large holes along 3-fold axes, but no significant channels along the fivefold directions. The opposite is true for AlMV, and in fact, the subunits of AlMV are tightly packed and closely interact about the 3-fold axes, while they form only the most tenuous fivefold contacts. While the $T=1$ particles of BMV are clearly made from pentameric units, the corresponding AlMV particles are likely formed from dimers aggregating about the 3-fold axes.[4,5,13,26]

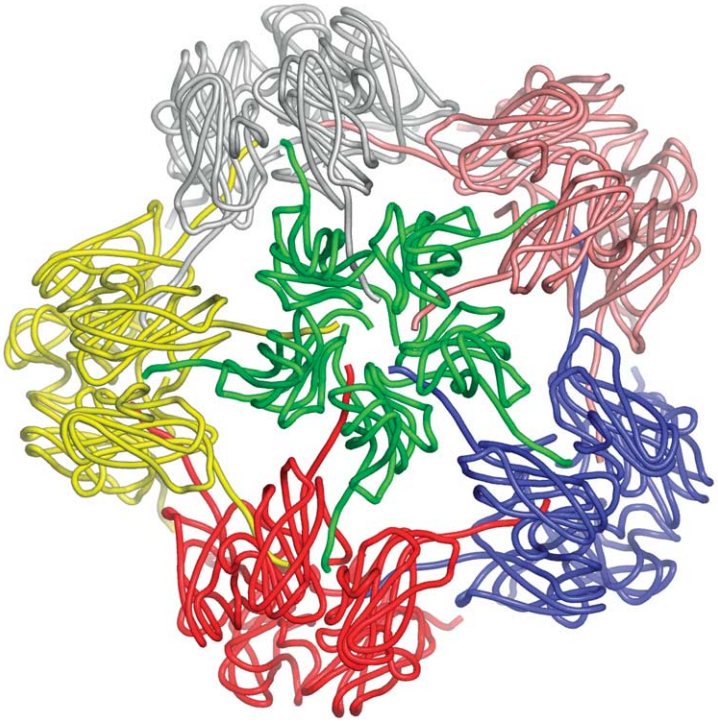

Figure 7. A hemisphere of the $T = 1$ particle of BMV viewed along a 5-fold axis showing the protrusion of pentamers from the surface. The structure is very open, with large channels along 3-fold axes. Pentamers are linked by extended carboxy terminal strands closely paired about icosahedral dyads between every adjacent pentamer.

Discussion

A quasi-icosahedral particle

Table 5 shows that the interfaces between particles are non-equivalent. We believe that these differential packing forces, in conjunction with the flexibility of the C-terminal inter-pentamer linkages, produce the quasi-icosahedral particle we observe. The flexible linkages allow the pentamers to tilt, expand outward or contract inward without disturbing the integrity of the pentamer. The "1/6" subunit relationships involving these linkages, found in Table 3, demonstrate this clearly. There is a 3.6 Å range in these spatial relationships. The B pentamer, which has the three

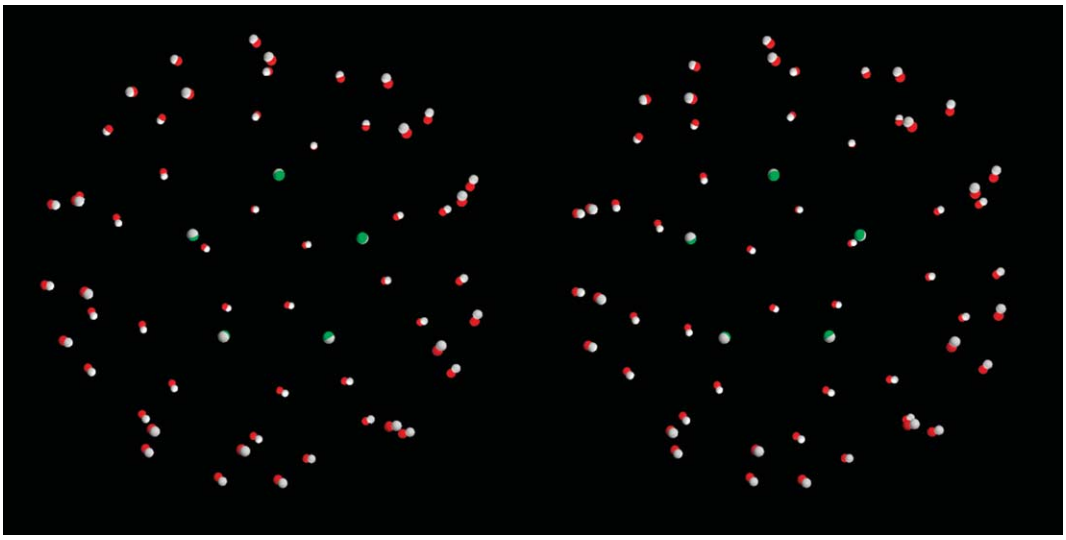

Figure 8. Stereo diagram of the centroids of the subunits (depicted as spheres) of both the icosahedral model (green and red) and the quasi-icosahedral model (white) with the corresponding pentamer of the former (green) superimposed on pentamer B of the latter model in the foreground. Most subunits of the quasi-icosahedral model have moved away from the icosahedral model by a counter-clockwise rotation around the 5-fold axis of pentamer B.

Table 4. Icosahedral distortions determined as the movement of pentamers going from a strict icosahedral particle to the quasi-icosahedral particle

A. *Results of superposition of icosahedral model onto quasi-icosahedral model*

Superposition group	Rotation (°)	Rotation axis with respect to 5-fold axis (°)	Translation (Å)	RMSD (Å)
Full particle	0.07	–	0.003	1.03
Pentamer A	2.09	91	0.68	0.43
Pentamer B	1.19	150	1.14	0.47
Pentamer C	0.97	89	0.59	0.44
Pentamer D	1.80	81	0.29	0.49
Pentamer E	1.78	87	0.39	0.45
Pentamer F	2.20	81	0.48	0.43

B. *Inter-axial angles between 5-fold axes*

C. *Inter-pentamer distances*[c]

Pair	Quasi-icosahedral[a] (°)	Quasi-icosahedral[b] (°)	Strict icosahedral[b] (°)	Quasi-icosahedral (Å)	Strict icosahedral (Å)
Adjacent	61.7–67.0	63.0–64.0	63.2–63.7	73.9–76.1	75.0–75.4
Intermediate	113.9–119.1	115.8–117.0	116.3–116.9	120.4–122.5	121.3–122.0
Opposite	175.6–178.5	179.4–179.9	180	142.4–143.6	142.6–143.2

D. *Radii from particle center to centroid*

	Quasi-icosahedral (Å)	Strict icosahedral (Å)
Pentamer	70.6–72.0	71.3–71.6
Subunit	74.2–76.2	75.1–75.5
Range per pentamer	0.5–1.7	0–0.2

The strict icosahedral model was superposed on the quasi-icosahedral model after which each pentamer was superposed on its equivalent pentamer in the quasi-icosahedral model. The translation is the distance between the pentamer centroids before and after superposition.

[a] The 5-fold axis for each pentamer was determined by averaging the 5-fold axes obtained from the superposition of every pair of subunits in each pentamer, a total of ten per pentamer.

[b] The angles were computed between vectors defined by the particle center and the centroids of the pentamers. For the strict icosahedral case, (a) and (b) are the same.

[c] These distances are between centroids of the pentamers.

shortest 1/6 translations (<7.3 Å), exhibits the greatest movement from its icosahedral position, has the smallest radial distance, and also has the most diverse packing interactions of any pentamer. So, surely, the flexibility of these linkages facilitates particle deformation. The many crystal forms, mentioned above, may be a result of different modes of particle deformation or lack of deformation. We presume that the same packing forces that cause the deformation also stabilize it so that uniform particles are maintained in the lattice.

We investigated the packing of the icosahedral model and found severe inter-particle contacts, especially at the B, D, E, and F pentamers. The A1, A3, C1, D5, and F3 subunits involved in packing of the quasi-icosahedral particle are not found within 4 Å of neighboring particles in the icosahedral model. On the other hand, subunit A5, not involved in the quasi-icosahedral packing, has a contact within 4 Å in the icosahedral case. Despite the deformation we see in this structure, we may find non-deformed particles in the other crystal forms and, indeed, particles free in solution may well, on average, have exact icosahedral symmetry, or be in structural equilibrium about the icosahedral ideal.

A model for the *T*=3 to *T*=1 transition

Earlier biochemical and physical analyses showed that when BMV was exposed to pH above 7, and/or to high NaCl or $CaCl_2$ concentrations, they first underwent a distinctive swelling transition and ultimately dissociated into a variety of products. After treatment with trypsin, which removed 63 amino acid residues from the N terminus, and subsequent dialysis, a variety of structures were obtained including $T=1$ icosahedral particles.[15,19,23,25,28,29,38] We later showed that a similar treatment with $CaCl_2$ and elevated pH, but absent any explicit trypsin treatment, produced $T=1$ particles, but that these were composed of protein subunits cleaved after amino acid 35.[14] Presumably, that cleavage was promoted by some endogenous protease in our BMV preparations. Using AFM, we were further able to show that, in the presence of high concentrations of $CaCl_2$, $T=3$ virions of BMV could directly transform into $T=1$ particles without undergoing complete dissociation.[14]

From these observations, and the now known structures of the initial and final particles, a picture begins to emerge of the transformation. This is illustrated in Figure 11. At pH>7 and in the

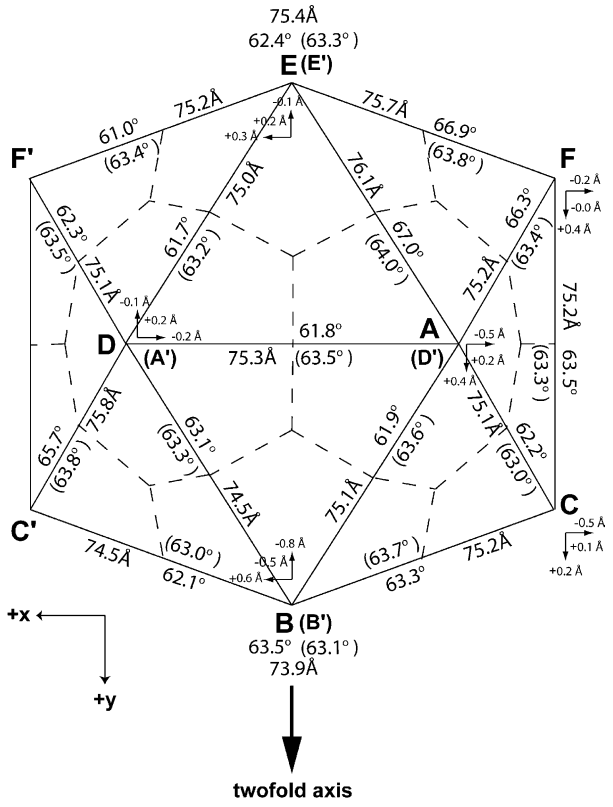

Figure 9. Diagram of the $T=1$ particle with the pentamers labeled as in Figure 4. Along the edges (inter-pentamer lines) are (a) the inter-axial angles (see note (1) of Table 4), (b) the angles (in parentheses) between the pentamer centroid-to-center vectors (see note (2) of Table 4), and (c) the inter-pentamer centroid-to-centroid distances. The inter-axial angles and inter-pentamer distances for the strict icosahedral structure are ~63.4° and ~75.2 Å, respectively. Next to each unique pentamer label are arrows indicating the direction and distance that that pentamer moved from the icosahedral model. The number between the arrows is the movement in the *z*-direction. The total distance each pentamer moved is listed in Table 4.

presence of salt, the native $T=3$ BMV virion in (a) begins swelling to assume a more open structure having a diameter about 15% larger.[23] This, it is believed,[25] allows access of both proteases and ribonuclease to the interior of the virion. Proteolytic cleavage and probably RNA degradation likely begin with (b), the swollen particle. As protein subunits are cleaved, they disengage from the RNA (which is simultaneously degraded or lost). There is also loss of Mg^{2+} from the quasi-3-fold axes where mutual repulsion of quasi-equivalent aspartic acid side-chains further promote dissociation. Because BMV virions are primarily maintained by protein–RNA interactions, and by divalent metal ions liganded by carboxyl clusters, this produces generalized instability.

From the AFM results, it appears that hexameric capsomeres are lost from the dissociating virions, but pentameric capsomeres are either not lost, or are lost to a lesser extent. As the hexamers are shed ((c) and (d)) condensation of the particles occurs as well. This contraction, however, must be accompanied by simultaneous rotation by 37° of the pentameric units remaining in the capsid, along with a conformational change in the C-terminal polypeptides of the coat proteins. The rearrangement of the C termini is crucial, as the termini are responsible for virtually all of the new capsid interactions that establish and maintain the $T=1$ architecture. Thus, while Figure 11 shows the $T=3$ to $T=1$ transformation as a series of events, this is undoubtedly an over simplification. Clearly, proteolysis, loss of ions, RNA degradation, loss of hexamers, rotation of pentamers, rearrangement of C termini, and condensation are all occurring more or less simultaneously but in some coordinated manner once swelling has occurred. New interactions between pentameric capsomeres through the C termini must be occurring simultaneously with loss of previous interactions between pentamers and hexamers. Were this not true, of course, the disrupted particles could not hold together and there could be no direct $T=3$ to $T=1$ particle transformation.

The C-terminal polypeptides

The C-terminal polypeptides of the coat proteins play a pivotal role in the transformation of $T=3$ virions into $T=1$ particles. Superficially, the interactions that the C-terminal peptides make between pentamers in the $T=1$ particles appear similar to those they make in the native virions, except that in the latter, the peptides join pentamer subunits to subunits in hexamers, or subunits in hexamers to those in neighboring hexamers. Dyad related C-terminal peptides are, however, quite near one another in the $T=1$ particle, but not in the native virion.

With the exception of the N-terminal peptides, the C-terminal peptides are the most conformationally variable segments of the entire coat protein when the A, B, and C subunits of a $T=3$ virion are compared. Thus, it is not unexpected that the C termini are even more varied in the $T=1$ particles. The sequence of this peptide is somewhat curious in that it has three phenylalanine residues, as well as other hydrophobic amino acid residues in the last ten. It is, therefore, probably capable of making a diverse range of hydrophobic interactions with adjacent subunits.

In the native virion, the C terminus of an A subunit is in closest contact with segments 177–185, 170–171, and amino acid 142 of a B subunit and at the same time with segments 128–133 and 146–150 of a C subunit. It would be risky to attempt identification of specific interactions in any more detail because of the relatively low resolution of the native BMV structure. In the $T=1$ particle, the extended C-terminal peptide contacts the underside of a subunit in a neighboring pentamer in quite a

Table 5. Subunits and residues at inter-particle interfaces that are within 4 Å of neighboring particles in the crystal lattice

A-B-C face		A′-B′-C′ face	
A3	A63, A161	C′1	D59
B1	S99, P163	B′5	A60, T62
B5	A60, T62	B′1	S99, P163
B5	A63, K64, A113	B′5	A63, K64, A113
C1	D59	A′3	A63, A161
A-E-F face		**B′-C-D′ face**	
A1	A60	C3	K64
E2	A60, I61, T62, N67	B′2	Q114, E116
F3	Q114	D′5	A63, K64
B-C′-D face		**A′-E′-F′ face**	
B2	Q114, E116	E′2	A60, I61, T62, N67
D5	A63, K64	F′3	Q114
C′3	K64	A′1	A60
D-E-F′ face		**D′-E′-F face**	
D3	T62, A63, K64	F1	T62, A63, K64, A65
E5	T62, A63, K64	E′5	T62, A63, K64
F′1	T62, A63, K64, A65	D′3	T62, A63, K64

The residues listed under each interface on the left of the table are in contact with the residues listed on the same line under the interface on the right of the Table.

different manner, with the nearest segments being 41–45, 50–53, 89–93, 131–134 and 172–177 of one subunit, residues 123, 132 and 138 of a second subunit, and five residues of three other subunits are within 4 Å of the C termini. Thus, the detailed interactions made by the C-terminal peptides are quite different in the $T=3$ and $T=1$ particles. It remains unclear whether the inherent versatility in making key, but different interactions in both $T=1$ and $T=3$ particles is just fortuitous, or has some functional significance.

Other researchers[15,16] have reported that $T=1$

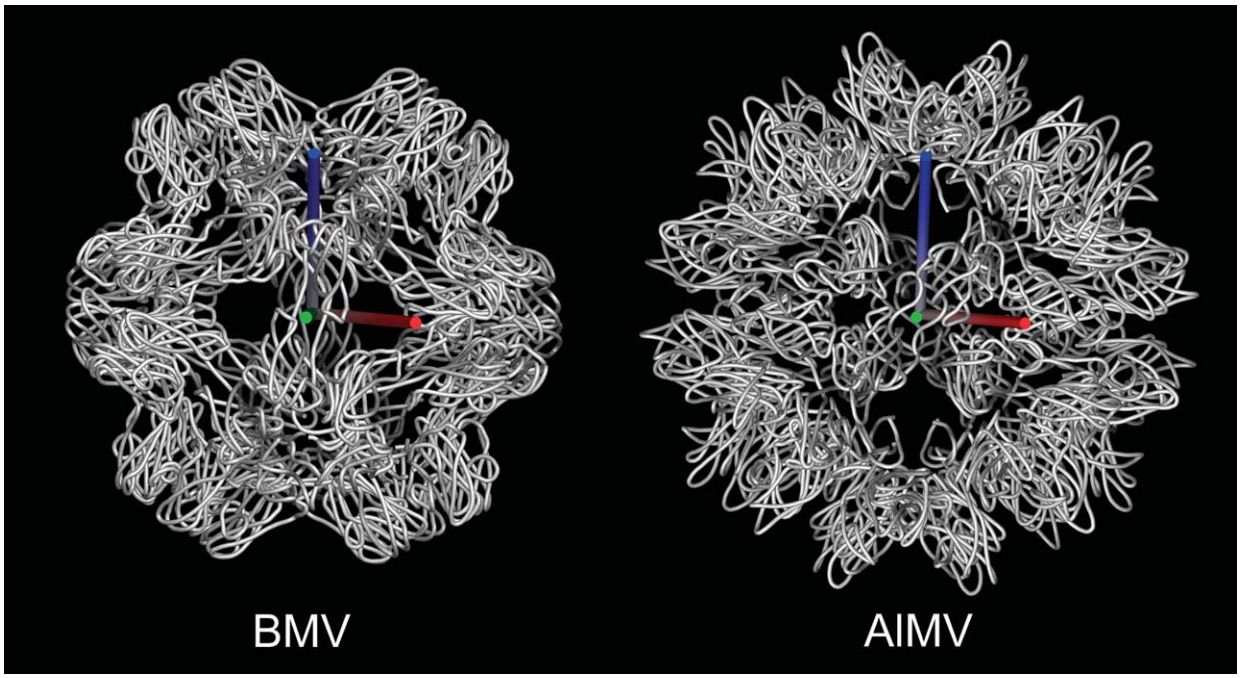

Figure 10. The $T=1$ BMV particle is shown at left and the $T=1$ particle from AlMV at right, both viewed along icosahedral dyad axes (shown in green). Both structures are open lattice works of protein subunits, but their architectures are quite different. While the BMV particle has large holes at 3-fold axes (shown in red), the particle from AlMV has broad channels along 5-fold axes (shown in blue). The BMV particle is made of discrete pentameric units, while that from AlMV has very little contact between pentameric subunits.

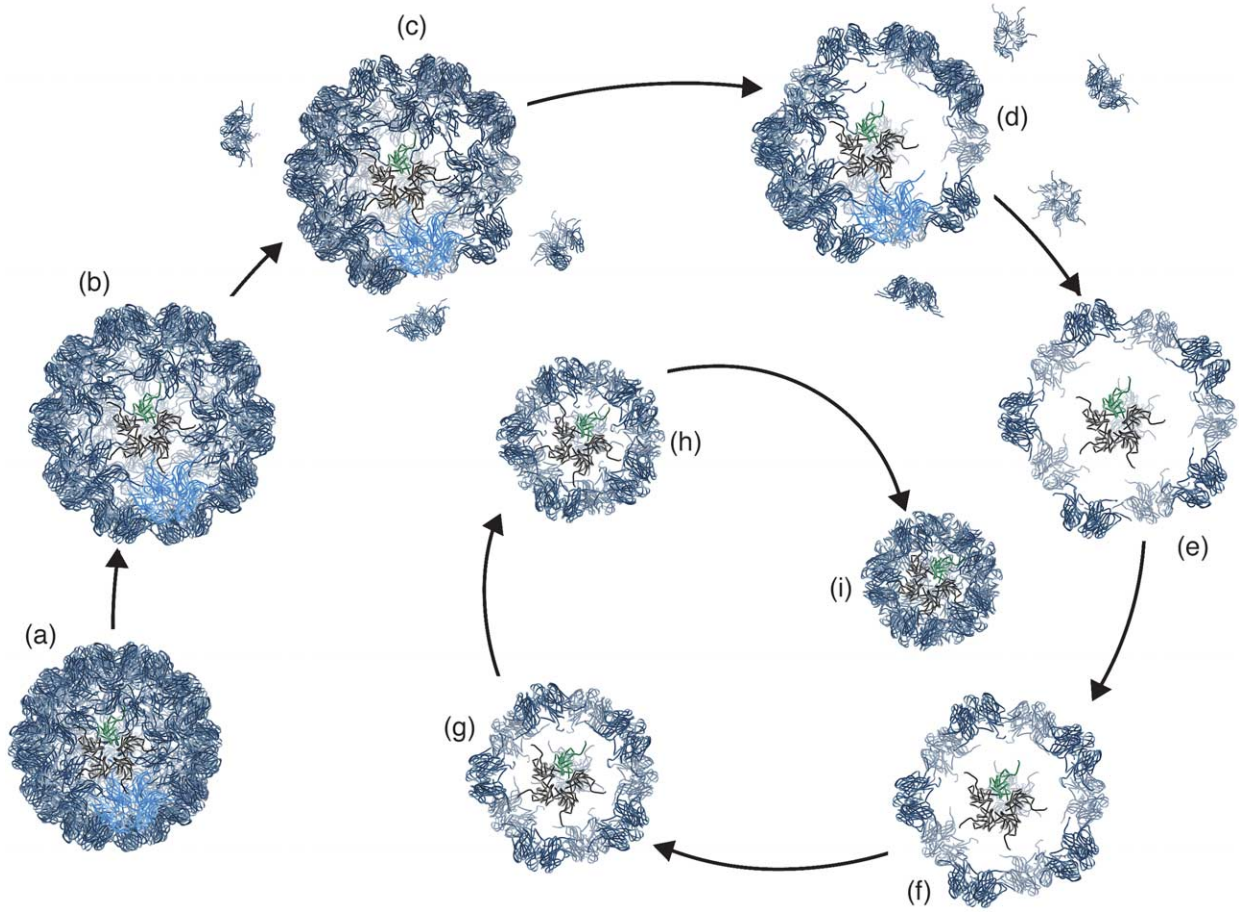

Figure 11. A diagram showing the sequence of events in the transformation of a native $T=3$ BMV virion in (a) into a $T=1$ particle (i). As a consequence of elevated pH and high-salt concentration, the native virion in (a) undergoes a transition to the swollen form in (b) thereby allowing exposure of the virion interior to proteases and ribonucleases. As proteolytic and nucleolytic cleavage proceeds, RNA fragments, amino terminal polypeptides, and hexameric units from the capsid are lost ((c)–(e)). As hexamers are lost, restructuring begins (e) as pentameric units start their 37° rotation, as they condense to the smaller particle. In (f)–(h) the pentamers continue their rotation as contraction of the assembly proceeds simultaneously.

particles derived from BMV can also be formed when treatment with trypsin effects cleavage between amino acid residues 63 and 64. This cleavage point would remove the first strand of the canonical β-barrel by cleaving at a β turn. The C termini in the $T=1$ structure we present here come into contact with amino acid residues 41–45 and 50–53 of a neighboring subunit, as well as additional amino acid residues on that, and other adjacent subunits. Were cleavage to have occurred after amino acid 63, then in that resulting $T=1$ particle, interactions involving amino acid residues 41–45 and 50–53 could not exist. Thus, subunit interactions in such a particle would be lessened, if they were otherwise the same, or they would have to be different to compensate for the loss.

T=1 particles of BMV and AlMV

The $T=1$ particles of AlMV and BMV, both bromoviruses, are, nevertheless, unlike one another in architecture and probably form by different mechanisms. Both, however, reflect the structures of their parent virions. In BMV, the $T=1$ particles are composed of the $T=3$ pentameric capsomeres, simply assembled using alternative interactions. The $T=1$ particles of AlMV show a similar character. Native AlMV particles, which are both spherical and bacilliform in shape, have a surface structure, as demonstrated by both transmission and cryo-electron microscopy, which is very similar to that in the $T=1$ AlMV particles.[26] Indeed, native AlMV capsids have subunits closely aggregated about the 3-fold axes, show strong dimer interactions across dyads, and exhibit a very open lattice permeated by large channels. Thus, it appears that, in both BMV and AlMV, many of the bonding properties of the capsid units inherent to the native virion are preserved, but that the final particle architecture is due to variation in interfacial contacts.

Particle transitions

Transition from an ordered $T=3$ particle, through partially ordered intermediates, to an ordered $T=1$ particle in the case of BMV, did not proceed by complete disassembly followed by self-reassembly. A distinctly different process occurred which involved the restructuring of the surface lattice of a transition particle. Restructuring of ordered, or partially ordered, surfaces is known to occur in other systems, most prominently, the surfaces of growing crystals[39–41] and the surfaces of micelles.[42,43] If such restructuring can take place in the transformation of the virions and particles studied here, then it may very well occur in natural virus assembly processes as well. That is, virus particles may not self-assemble in a sequentially ordered manner, but may first form some less ordered intermediate, which then restructures to create the exact icosahedral organization that we observe in the native particle.

Materials and Methods

Preparation of the *T*=1 particles

BMV was obtained from Professor A.L. Rao at the University of California at Riverside and infected into young barley plants (*H. vulgare cv. Dickson*). It was purified from mature plants as described by Adolph[44] with some minor modifications described in Lucas *et al*.[14] The final stages of the procedure included purification on a CsCl gradient, dialysis, and concentration to about 7 mg/ml (the concentration used for the crystallization of the intact virus). Throughout these procedures the pH was maintained below pH 5.0

$T=1$ particles of BMV were produced by a modification of the conventional procedure of Choi *et al*.,[30] but no extraneous trypsin or other protease was added to the BMV preparation. Bovine RNase A was from Sigma Co. (St Louis). Details of the procedure are given in Lucas *et al*.[14] SDS-PAGE and analysis by mass spectrometry showed the coat protein to be an abbreviated form of the wild-type protein and to have arisen from proteolytic cleavage between amino acid residues 35 and 36.[14]

Crystallization

Polyhedral crystals of the $T=1$ BMV particles as large as 0.5 mm on edge were grown for X-ray diffraction analysis using conventional procedures. These utilized vapor diffusion in Cryschem sitting drop plates (Hampton Research, Aliso Viejo, CA) using drop volumes of 6–10 μl. Optimal conditions were identified, and these were droplets composed of equal volumes of the particle solution and 2.1 M sodium malonate[45] at pH 7.5. Reservoirs of 0.65 ml of the 2.1 M malonate were equilibrated with the microdrops at room temperature for approximately two to four weeks before crystals were harvested.

Data collection

Data were collected on beamline 5.0.1 at the Advanced Light Source (ALS) at the Lawrence Berkeley National Laboratory using a wavelength of 1.1 Å and a two by two CCD detector (SDMS, San Diego, CA). The crystals were cryogenically frozen directly from their mother liquor, the malonate serving as the necessary cryo-protectant as well as the crystallization salt. Oscillation increments were 0.5° with exposure times of 120 seconds. The crystal to detector distance was 250.4 mm. Data were processed to a resolution of 2.9 Å and merged using the programs DENZO/SCALEPACK.[46] The data was 99.5% complete to 2.9 Å resolution with 100% completeness in the outermost shell (2.90–3.00 Å). The R_{merge} for all data was 0.153 with an average redundancy of 18.9 for space group $P4_322$. An example of the diffraction pattern for these crystals was shown by Lucas *et al*.[14]

Structure solution, refinement and analysis

Self-rotation functions with 4, 5, and 6 Å data using CNS[47] provided the initial particle orientation. The initial structure solution was obtained by molecular replacement using dimers, trimers, or pentamers of the native $T=3$ BMV model. An X-PLOR[48–50] script was written in which these BMV assemblies were incrementally contracted along the appropriate icosahedral symmetry axis, rotated about that axis, as well as translated along and rotated around the crystallographic *y*-axis in space group $P4_122$. At each incremental change in the model, the correlation coefficient (CC) and *R*-factor were computed. Still assuming space group $P4_122$, a model composed of a hemisphere of six pentamers, corresponding to the crystallographic asymmetric unit, was constructed. This model was rotated about and translated along the *y*-axis incrementally to refine the particle orientation and position, calculating CC and *R* at each increment. This procedure was repeated for space groups $P4_1$ and $P4_3$ using a full particle model.

An adaptation of the density modification script in CNS[47] was used to perform phase extension utilizing the icosahedral non-crystallographic symmetry operators for map averaging. The molecular replacement models were used to calculate phases to 10 Å and to make averaging and solvent masks, using the program MAMA.[51] For space groups $P4_122$ and $P4_322$, 30-fold NCS averaging was performed while, for space groups $P4_1$ and $P4_3$, 60-fold NCS averaging was executed.

Model rebuilding was accomplished with the program "O".[52] All model refinement was performed with the program CNS using the maximum likelihood target based on observed intensities; no experimental phase information was employed. Ultimately, the strict icosahedral symmetry was released and the 30 subunits of the $T=1$ particle were refined under NCS restraints only. The best NCS restraints were determined as those restraints that produced the lowest R_{free} after refinement. These restraints are described in Table 2 along with some refinement and model statistics.

A comparison of the spatial arrangements of subunits across icosahedral and quasi-symmetry elements was made as follows. The $T=3$ subunit pair (e.g., A_1/B_5) was superimposed onto the corresponding $T=1$ pair (1/6) utilizing the C^{α} atoms of residues 41–181 of subunit A_1. The residual rotation and translations were then determined from the superposition of subunit B_5 onto subunit 6 of the $T=1$ particle. This differs from the method used in the calculations for SeMV in that the initial superposition in SeMV was performed for the subunit pair, not just a single subunit, followed by superposition of the second subunit to obtain the residual rotation and translation results. Due to the extreme changes in the

BMV transition from $T=3$ to $T=1$, our method seems more appropriate. Because of the relatively benign changes between the $T=3$ and $T=1$ SeMV particles, the differences between the two methods may be minimal for SeMV.

Figures 1, 4, 6, and 9 were made with Adobe Illustrator.† Figure 2 was produced with Microsoft Excel.‡ Figure 5 was generated with MOLSCRIPT[53] and Raster3D.[54] Figures 7, 8 and 10 were produced with PyMol.[55] Figures 3 and 10 were created with PyMol[55] and Adobe Illustrator.†

Protein Data Bank accession code

The coordinates have been deposited in the RCSB Protein Data Bank under code 1YC6.

Acknowledgements

This research was supported by grant GM58868-02 from the NIH. The authors thank Aaron Greenwood for preparing the illustrations, and the staff at the Advanced Light Source in Berkeley, CA for their capable assistance.

References

1. Rao, A. L. N. & Grantham, G. L. (1995). Biological significance of the seven amino-terminal basic residues of brome mosaic virus coat protein. *Virology*, **211**, 42–52.
2. Schmitz, I. & Rao, A. L. N. (1998). Deletions in the conserved amino-terminal basic arm of cucumber mosaic virus coat protein disrupt virion assembly but do not abolish infectivity and cell-to-cell movement. *Virology*, **248**, 323–331.
3. Murphy, F. A., Fauquet, C. M., Bishop, D. H. L., Ghabrial, S. A., Jarvis, A. W., Martelli, G. P. *et al.* (1995). Editors of *Virus Taxonomy*, Springer-Verlag, Vienna, Austria.
4. Kumar, A., Reddy, V. S., Yusibov, V., Chipman, P. R., Hata, Y., Fita, I. *et al*. (1997). The structure of alfalfa mosaic virus capsid protein assembled as a $T=1$ icosahedral particle at 4.0 A resolution. *J. Virol.* **71**, 7911–7916.
5. Jaspars, E. M. J. (1985). Interaction of alfalfa mosaic virus nucleic acid and protein. In *Molecular Plant Virology* (W, D. J., ed.), vol. I, pp. 155–221, CRC Press, Inc, Boca Raton, FL.
6. Van Vloten-Doting, L., Francki, R. I. B., Fulton, R. W., Kaper, J. M. & Lane, L. C. (1981). Tricornaviridae: a proposed family of plant viruses with tripartite, single-stranded RNA genomes. *Intervirology*, **15**, 198–203.
7. Savithri, H. S. & Erickson, J. W. (1983). The self-assembly of the cowpea strain of southern bean mosaic virus: formation of $T=1$ and $T=3$ nucleoprotein particles. *Virology*, **126**, 328–335.
8. Erickson, J. W. & Rossmann, M. G. (1982). Assembly and crystallization of a $T=1$ icosahedral particle from trypsinized southern bean mosaic virus coat protein. *Virology*, **116**, 128–136.
9. Erickson, J. W., Silva, A. M., Murthy, M. R. N., Fita, I. & Rossmann, M. G. (1985). The structure of a $T=1$ icosahedral empty particle from southern bean mosaic virus. *Science*, **229**, 625–629.
10. Sangita, V., Lokesh, G. L., Satheshkumar, P. S., Vijay, C. S., Saravanan, V., Savithri, H. S. & Murthy, M. R. N. (2004). $T=1$ capsid structures of sesbania mosaic virus coat protein mutants: determinants of $T=3$ and $T=1$ capsid assembly. *J. Mol. Biol.* **342**, 987–999.
11. Sangita, V., Parthasarathy, S., Toma, S., Lokesh, G. L., Gowri, T. D. S., Satheshkumar, P. S. *et al*. (2002). Determination of the structure of the recombinant $T=1$ capsid of sesbania mosaic virus. *Curr. Sci.* **82**, 1123–1131.
12. Abdel-Meguid, S. S., Fukuyama, K. & Rossmann, M. G. (1982). The orientation of a $T=1$ assembly of alfalfa mosaic virus coat protein in a hexagonal crystalline array. *Acta Crystallog. sect. B*, **38**, 2004–2008.
13. Fukuyama, K., Abdel-Meguid, S. S., Johnson, J. E. & Rossmann, M. G. (1983). Structure of a $T=1$ aggregate of alfalfa mosaic virus coat protein seen at 4.5 Å resolution. *J. Mol. Biol.* **167**, 873–894.
14. Lucas, R. W., Kuznetsov, Y. G., Larson, S. B. & McPherson, A. (2001). Crystallization of brome mosaic virus and $T=1$ brome mosaic virus particles following a structural transition. *Virology*, **286**, 290–303.
15. Cuillel, M., Jacrot, B. & Zulauf, M. (1981). A $T=1$ capsid formed by the protein of brome mosaic virus in the presence of trypsin. *Virology*, **110**, 63–72.
16. Bol, J. F., Kraal, B. & Brederode, F. T. (1974). Limited proteolysis of alfalfa mosaic virus: influence on the structural and biological function of the coat protein. *Virology*, **58**, 101–110.
17. Bancroft, J. B., Hills, G. J. & Markham, R. (1967). A study of the self-assembly process in a small spherical virus. Formation of organized structures from protein subunits *in vitro*. *Virology*, **31**, 354–379.
18. Bancroft, J. B., Bracker, C. E. & Wagner, G. W. (1969). Structures derived from cowpea chlorotic mottle and brome mosaic virus protein. *Virology*, **38**, 324–335.
19. Pfeiffer, P. & Hirth, L. (1974). Aggregation states of brome mosaic virus protein. *Virology*, **61**, 160–167.
20. Lane, L. C. (1977). Brome Mosaic Virus. *CMI/AAB Descript. Plant Viruses*. **180**, 1–4.
21. Van Regenmortel, M. H. V., Fauquet, C. M., Bishop, D. H. L., Carstens, E. B., Estes, M. K., Lemon, S. M. *et al*. (2000). *Virus Taxonomy: Seventh Report of the International Committee on Taxonomy of Viruses*, pp. 923–928, Academic Press, San Diego.
22. Ahlquist, P., Allison, R., Dejong, W., Janda, M., Kroner, P., Pacha, R. & Traynor, P. (1990). Molecular biology of bromovirus replication and host specificity. In *Viral Genes and Plant Pathogenesis* (Pirone, T. P. & Shaw, J. G., eds), pp. 144–155, Springer-Verlag, New York.
23. Chauvin, C., Pfeiffer, P., Witz, J. & Jacrot, B. (1978). Structural polymorphism of bromegrass mosaic virus: a neutron small angle scattering investigation. *Virology*, **88**, 138–148.
24. Lucas, R. W., Larson, S. B. & McPherson, A. (2002). The crystallographic structure of brome mosaic virus. *J. Mol. Biol.* **317**, 95–108.
25. Kaper, J. M. (1975). The chemical basis of virus structure, dissociation and reassembly. *Frontiers Biol.* **39**, 1–485.

† Adobe Illustrator, 10.0 edit., Adobe Systems Inc.
‡ Microsoft Excel, Microsoft Corp.

26. Johnson, J. E. & Argos, P. (1985). Virus particle stability and structure. In *The Plant Viruses* (Francki, R. I. B., ed.), vol. 1, Plenum Press, New York.
27. Anderegg, J. W., Wright, M. & Kaesberg, P. (1963). An X-ray scattering study of bromegrass mosaic virus. *Biophys. J.* **3**, 175–182.
28. Pfeiffer, P., Herzog, M. & Hirth, L. (1976). RNA viruses: stabilization of brome mosaic virus. *Philos. Trans. Roy. Soc. Lond. B. Biol. Sci.* **276**, 99–107.
29. Bancroft, J. B. & Hiebert, E. (1967). Formation of an infectious nucleoprotein from protein and nucleic acid isolated from a small spherical virus. *Virology*, **32**, 354–356.
30. Choi, Y. G., Grantham, G. L. & Rao, A. L. (2000). Molecular studies on bromovirus capsid protein. *Virology*, **270**, 377–385.
31. Lucas, R. W., Larson, S. B., Canady, M. A. & McPherson, A. (2002). The structure of tomato aspermy virus by X-ray crystallography. *J. Struct. Biol.* **139**, 90–102.
32. Canady, M. A., Larson, S. B., Day, J. & McPherson, A. (1996). Crystal structure of turnip yellow mosaic virus. *Nature Struct. Biol.* **3**, 771–781.
33. Larson, S. B., Koszelak, S., Day, J., Greenwood, A., Dodds, J. A. & McPherson, A. (1993). Three-dimensional structure of satellite tobacco mosaic virus at 2.9 Å resolution. *J. Mol. Biol.* **231**, 375–391.
34. Larson, S. B., Day, J., Canady, M. A., Greenwood, A. & McPherson, A. (2000). Refined structure of desmodium yellow mottle tymovirus at 2.7 Å resolution. *J. Mol. Biol.* **301**, 625–642.
35. Laskowski, R. A., MacArthur, M. W., Moss, D. S. & Thornton, J. M. (1993). PROCHECK: a program to check the stereochemical quality of protein structures. *J. Appl. Crystallog.* **26**, 283–291.
36. Ban, N., Larson, S. B. & McPherson, A. (1995). Structural comparison of the plant satellite viruses. *Virology*, **214**, 571–583.
37. Wu, C. H., Huang, H., Arminski, L., Castro-Alvear, J., Chen, Y., Hu, Z. Z. *et al*. (2002). The Protein Information Resource: an integrated public resource of functional annotation of proteins. *Nucl. Acids Res.* **30**, 35–37.
38. Bancroft, J. B., Hiebert, E. & Bracker, C. E. (1969). The effects of various polyanions on shell formation of some spherical viruses. *Virology*, **39**, 924–930.
39. den Nijs, M. (1994). Roughening, preroughening, and reconstruction transitions in crystal surfaces. In *The Chemical Physics of Solid Surfaces and Heterogeneous Catalysis* (King, D. A. & Woodruff, D. P., eds), vol. 7, Elsevier, Amsterdam.
40. Pimpinelli, A. & Villain, J. (1998). *Physics of Crystal Growth*, Cambridge University Press, Cambridge.
41. Li, H., Perozzo, M. A., Konnert, J. H., Nadarajah, A. & Pusey, M. L. (1999). Determining the molecular-packing arrangements on protein crystal faces by atomic force microscopy. *Acta Crystallog. sect. D*, **55**, 1023–1035.
42. Gelbart, W. M., Ben-Shaul, A. & Roux, D. (1994). *Micelles, Membranes, Microemulsions and Monolayers*, Springer-Verlag, New York.
43. Moroi, Y. (1992). *Micelles: Theoretical and Applied Aspects*, Plenum Press, New York.
44. Adolph, K. W. (1994). *Molecular Virology Techniques Methods in Molecular Genetics*, vol. 4, Academic Press, San Diego.
45. McPherson, A. (2001). A comparison of salts for the crystallization of macromolecules. *Protein Sci.* **10**, 418–422.
46. Otwinowski, Z. & Minor, W. (1997). Processing of X-ray diffraction data collected in oscillation mode. In *Macromolecular Crystallography* (Carter, J. W. M. J. & Sweet, R. M., eds), Academic Press, San Diego.
47. Brunger, A. T., Adams, P. D., Clore, G. M., DeLano, W. L., Gros, P., Grosse-Kunstleve, R. W. *et al*. (1998). Crystallography & NMR system: a new software suite for macromolecular structure determination. *Acta Crystallog. sect. D*, **54**, 905–921.
48. Brunger, A. T., Kuriyan, J. & Karplus, M. (1987). Crystallographic R factor refinement by molecular dynamics. *Science*, **235**, 458–460.
49. Brunger, A. T. (1991). Simulated annealing in crystallography. *Annu. Rev. Phys. Chem.* **42**, 197–223.
50. Brunger, A. T. (1992). The free *R* value: a novel statistical quantity for assessing the accuracy of crystal structures. *Nature*, **355**, 427–474.
51. Kleywegt, G. J. & Jones, A. T. (1993). Masks made easy. *CCP4/ESF-EACBM Newsletter Protein Crystallog.* **28**, 56–59.
52. Jones, A. T. & Kjeldgaard, M. (1994). O-The Manual, Version 5.10, Uppsala University Press, Uppsala.
53. Kraulis, P. J. (1991). MOLSCRIPT: a program to produce both detailed and schematic plots of protein structures. *J. Appl. Crystallog.* **24**, 946–950.
54. Merrit, E. A. & Murphy, M. E. P. (1994). Raster3D version 2.0.A program for photorealistic molecular graphics. *Acta Crystallog. sect. D*, **50**, 869–873.
55. DeLano, W. L. (2002). *The PyMol Molecular Graphics System*, DeLano Scientific, San Carlos, CA.

Edited by I. Wilson

(Received 4 May 2004; received in revised form 2 December 2004; accepted 3 December 2004)